

Sizable triple Higgs couplings in the 2HDM: Prospects for future e^+e^- colliders*

F. ARCO^{1,2†‡}, S. HEINEMEYER^{2,3,4§} AND M.J. HERRERO^{1,2¶}

¹*Departamento de Física Teórica, Universidad Autónoma de Madrid,
Cantoblanco, 28049, Madrid, Spain*

²*Instituto de Física Teórica (UAM/CSIC), Universidad Autónoma de Madrid,
Cantoblanco, 28049, Madrid, Spain*

³*Campus of International Excellence UAM+CSIC, Cantoblanco, 28049, Madrid, Spain*

⁴*Instituto de Física de Cantabria (CSIC-UC), 39005, Santander, Spain*

Abstract

In the framework of the \mathcal{CP} conserving Two Higgs Doublet Model (2HDM), type I and II, we study the triple Higgs couplings with at least one light h Higgs boson that is identified by the 125 GeV Higgs boson. We define benchmark planes that exhibit large values of triple Higgs couplings, while being in agreement with all experimental and theoretical constraints. Finally, we analyze the impact of the triple Higgs couplings on the production cross section of two neutral Higgs bosons in two channels, $\sigma(e^+e^- \rightarrow h_i h_j Z)$ and $\sigma(e^+e^- \rightarrow h_i h_j \nu \bar{\nu})$ with $h_i h_j = hh, hH, HH, AA$. We show that the triple Higgs couplings have an important impact on these e^+e^- production cross sections.

*Talk presented at the International Workshop on Future Linear Colliders (LCWS2021), 15-18 March 2021. C21-03-15.1

†Speaker

‡email: Francisco.Arco@uam.es

§email: Sven.Heinemeyer@cern.ch

¶email: Maria.Herrero@uam.es

1 Introduction

The discovery of a Higgs boson at ATLAS and CMS in 2012 was a milestone in high-energy physics [1, 2]. Within theoretical and experimental uncertainties this new particle is consistent with the existence of a Standard-Model (SM) Higgs boson at a mass of ~ 125 GeV [3]. The measurements of Higgs-boson couplings, which are known experimentally to a precision of roughly $\sim 20\%$, leave room for Beyond Standard-Model (BSM) interpretations. Many BSM models possess extended Higgs-boson sectors. While no sign of BSM physics was (yet) discovered at the LHC, one of the main tasks of the LHC Run III and beyond is to determine whether the particle forms part of the Higgs sector of an extended model.

The measurement of the trilinear Higgs coupling of the SM-like Higgs boson λ_{hhh} is a key element in the investigation of the Higgs-boson sector. (see Refs. [4, 5] for recent reviews on Higgs couplings measurements at future colliders). In the case of a BSM Higgs-boson sector, equally important is the measurement of BSM trilinear Higgs-boson couplings. So far, most experimental studies have assumed the SM value of λ_{hhh} . In BSM models, however, this coupling may differ significantly from its SM value. The expected precision that can be achieved at different future colliders in the measurement of λ_{hhh} can depend strongly on the value realized in nature.

A natural extension of the Higgs-boson sector of the SM is the “Two Higgs Doublet Model” (2HDM) (see, e.g., [6–8] for reviews). The 2HDM contains five physical Higgs bosons: the light and the heavy \mathcal{CP} -even h and H , the \mathcal{CP} -odd A , and the pair of charged Higgs bosons, H^\pm . The two mixing angles α and β diagonalize the \mathcal{CP} -even and \mathcal{CP} -odd Higgs boson sector, respectively. The parameter $\tan\beta$ is defined by the ratio of the two vacuum expectation values, $\tan\beta := v_2/v_1$.

We review the allowed ranges for all triple Higgs couplings involving at least one light, SM-like Higgs boson. Specifically: λ_{hhh} , λ_{hhH} , λ_{hHH} , λ_{hAA} and $\lambda_{hH^+H^-}$ [9]. It is assumed that the light \mathcal{CP} -even Higgs-boson h is SM-like with a mass of $m_h \sim 125$ GeV. All other Higgs bosons are assumed to be heavier. To avoid flavor changing neutral currents at the tree-level, a Z_2 symmetry is imposed [10]. This symmetry is possibly softly broken by the parameter m_{12}^2 . Four types of the 2HDM can be realized, depending on how this symmetry is extended to the fermion sector: type I and II, lepton specific and flipped [7]. In the 2HDM also the stability conditions for the Higgs potential change with respect to the SM [11] (for a review see [12]). Here (as in Ref. [9]) we focus on the 2HDM type I and II. The allowed ranges for the triple Higgs couplings are obtained taking into account: the theoretical constraints from unitarity and stability (we use [12–14]), the experimental production and decay rates of the SM-like Higgs boson (we use `HiggsSignals` [20–22]), experimental constraints from direct Higgs-boson searches (we use `HiggsBounds` [15–19]), as well as flavor observables (we use `SuperIso` [23, 24], complemented with [25–27]) and electroweak precision observables (EWPO) (we use the S , T and U parameters [28, 29], complemented with [30, 31] and bounds from [32]).

The main interest in the ranges allowed for the triple Higgs-boson couplings is the fact that they affect the rates of multi-Higgs boson production at current and future colliders. Within the 2HDM, the production of Higgs boson pairs like hh , hH , HH , hH^\pm , AA and H^+H^- can be significantly affected by (large) values of triple Higgs couplings, which are yet allowed by the present constraints. At e^+e^- colliders two different channels are of interest:

$e^+e^- \rightarrow h_i h_j Z$ and $e^+e^- \rightarrow h_i h_j \nu \bar{\nu}$ with $h_i h_j = hh, hH, HH$ and AA . The first one is similar to the ‘‘Higgs-strahlung’’ channel of single Higgs production. The second one has an important contribution from the vector-boson fusion mediated subprocess, $W^+W^- \rightarrow h_i h_j$, where the WW pairs (virtual, in general) are radiated from the initial e^+e^- together with the neutrinos: $e^+e^- \rightarrow W^*W^* \nu \bar{\nu}$. The latter processes also receives a contribution from the Z mediated subprocess, $e^+e^- \rightarrow Zh_i h_j$, with $Z \rightarrow \nu \bar{\nu}$, which is usually smaller than the contribution from WW fusion at the high energy colliders.

2 The Model and the constraints

2.1 The Two Higgs Doublet Model

We work within the \mathcal{CP} conserving 2HDM. The scalar potential of this model is given by [8]:

$$\begin{aligned} V = & m_{11}^2(\Phi_1^\dagger \Phi_1) + m_{22}^2(\Phi_2^\dagger \Phi_2) - m_{12}^2(\Phi_1^\dagger \Phi_2 + \Phi_2^\dagger \Phi_1) + \frac{\lambda_1}{2}(\Phi_1^\dagger \Phi_1)^2 + \frac{\lambda_2}{2}(\Phi_2^\dagger \Phi_2)^2 \\ & + \lambda_3(\Phi_1^\dagger \Phi_1)(\Phi_2^\dagger \Phi_2) + \lambda_4(\Phi_1^\dagger \Phi_2)(\Phi_2^\dagger \Phi_1) + \frac{\lambda_5}{2}[(\Phi_1^\dagger \Phi_2)^2 + (\Phi_2^\dagger \Phi_1)^2], \end{aligned} \quad (1)$$

where Φ_1 and Φ_2 denote the two $SU(2)_L$ doublets. As mentioned above, the occurrence of tree-level flavor changing neutral currents (FCNC) is avoided by imposing a Z_2 symmetry on the scalar potential. The scalar fields transform as:

$$\Phi_1 \rightarrow \Phi_1, \quad \Phi_2 \rightarrow -\Phi_2. \quad (2)$$

The Z_2 symmetry, however, is softly broken by the m_{12}^2 term in the Lagrangian. The extension of the Z_2 symmetry to the Yukawa sector avoids tree-level FCNCs. Depending on the Z_2 parities of the fermions, this results in four variants of 2HDM: type I, type II, lepton-specific (or type X) and flipped (or type Y) [7].

Taking the electroweak symmetry breaking (EWSB) minima to be neutral and \mathcal{CP} -conserving, the scalar fields after EWSB can be parameterized as:

$$\Phi_1 = \begin{pmatrix} \phi_1^+ \\ \frac{1}{\sqrt{2}}(v_1 + \rho_1 + i\eta_1) \end{pmatrix}, \quad \Phi_2 = \begin{pmatrix} \phi_2^+ \\ \frac{1}{\sqrt{2}}(v_2 + \rho_2 + i\eta_2) \end{pmatrix}. \quad (3)$$

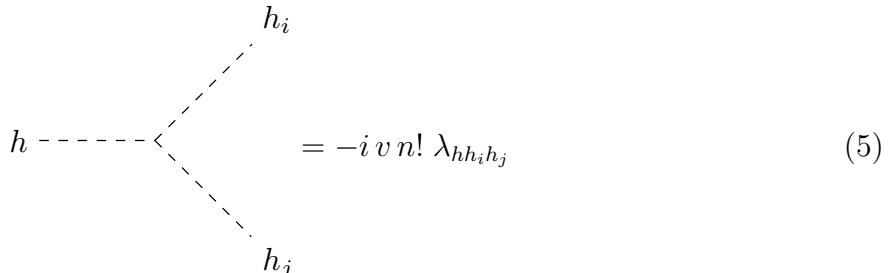
Here v_1, v_2 are the real vevs acquired by the fields Φ_1, Φ_2 , respectively, and $\tan \beta := v_2/v_1$. They satisfy the relation $v = \sqrt{(v_1^2 + v_2^2)}$, with $v \simeq 246$ GeV being the SM vev. There are eight degrees of freedom in the fields $\phi_{1,2}^\pm, \rho_{1,2}$ and $\eta_{1,2}$. They give rise to three Goldstone bosons, G^\pm and G^0 , and five massive physical scalar fields: two \mathcal{CP} -even scalar fields, h and H , one \mathcal{CP} -odd one, A , and one charged pair, H^\pm . Here the mixing angles α and β diagonalize the CP-even and -odd Higgs boson sectors, respectively.

After the consideration of the minimization conditions, the 2HDM can be characterized by seven free parameter. The 2HDM is studied in the physical basis, where the free parameters of the model, which we use as input, are chosen as:

$$c_{\beta-\alpha}, \quad \tan \beta, \quad v, \quad m_h, \quad m_H, \quad m_A, \quad m_{H^\pm}, \quad m_{12}^2, \quad (4)$$

where we use the short-hand notation $s_x = \sin(x)$, $c_x = \cos(x)$. The analysis identifies the lightest \mathcal{CP} -even Higgs boson, h , with the one observed at ~ 125 GeV.

The potential of the 2HDM defines the interactions in the scalar sector. Here we focus on the couplings of the lightest \mathcal{CP} -even Higgs boson with the other BSM bosons: λ_{hhh} , λ_{hhH} , λ_{hHH} , λ_{hAA} and $\lambda_{hH^+H^-}$. These $\lambda_{hh_ih_j}$ couplings are defined such that the Feynman rules are given by:



$$= -i v n! \lambda_{hh_ih_j} \quad (5)$$

Here n is the number of identical particles in the vertex, and we adopt this notation so the light Higgs trilinear has the same definition as in the SM, i.e. $-6iv\lambda_{\text{SM}}$ with $\lambda_{\text{SM}} = m_h^2/2v^2 \simeq 0.13$.

It should be noted that all the couplings of the \mathcal{CP} -even Higgs bosons strongly depend on $c_{\beta-\alpha}$. For $c_{\beta-\alpha} = 0$ one recovers all the interactions of the SM Higgs boson for the h state, which is called the *alignment limit*. This limit is very important since the Higgs measurements in colliders seem to overall agree with the SM values, see the discussion in the next subsection.

2.2 Constraints

Here we briefly list the experimental and theoretical constraints that were employed in the analysis (more details can be found in Ref. [9]).

- **Constraints from electroweak precision data**

Constraints from the electroweak precision observables (EWPO) can for “pure” Higgs-sector extensions of the SM, be expressed in terms of the oblique parameters S , T and U [28, 29]. In the 2HDM the T parameter is most constraining and requires either $m_{H^\pm} \approx m_A$ or $m_{H^\pm} \approx m_H$. In Ref. [9] we explored three scenarios: (A) $m_{H^\pm} = m_A$, (B) $m_{H^\pm} = m_H$ and (C) $m_{H^\pm} = m_A = m_H$. Here we will focus on scenario C. For the evaluation of the T parameter we use the code 2HDMC-1.8.0 [33].

- **Theoretical constraints**

Here the important constraints come from tree-level perturbative unitarity and stability of the vacuum. They are ensured by an explicit test on the underlying Lagrangian parameters, see Ref. [9] for details. The parameter space allowed by these two constraints can be enlarged, in particular to higher BSM Higgs-boson mass values by the condition,

$$m_{12}^2 = \frac{m_H^2 \cos^2 \alpha}{\tan \beta} . \quad (6)$$

- **Constraints from direct searches at colliders**

The 95% confidence level exclusion limits of all important searches for BSM Higgs bosons are included in the public code `HiggsBounds v. 5.9` [15–19], including Run 2 data from

the LHC. Given a set of theoretical predictions in a particular model, `HiggsBounds` determines which is the most sensitive channel and determines, based on this most sensitive channel, whether the point is allowed or not at the 95% CL. As input the code requires some specific predictions from the model, like branching ratios or Higgs couplings, that we computed with the help of `2HDMC` [33].

- **Constraints from the SM-like Higgs-boson properties**

Any model beyond the SM has to accommodate the SM-like Higgs boson, with mass and signal strengths as they were measured at the LHC. In our scans the compatibility of the \mathcal{CP} -even scalar h with a mass of 125.09 GeV with the measurements of signal strengths at Tevatron and LHC is checked with the code `HiggsSignals v.2.6` [20–22]. `HiggsSignals` provides a statistical χ^2 analysis of the SM-like Higgs-boson predictions of a certain model compared to the measurement of Higgs-boson signal rates and masses from Tevatron and LHC. Again, the predictions of the 2HDM have been obtained with `2HDMC` [33]. Here, as in Ref. [9], we will require that for a parameter point of the 2HDM to be allowed, the corresponding χ^2 is within 2σ ($\Delta\chi^2 = 6.18$) from the SM fit.

- **Constraints from flavor physics**

Constraints from flavor physics have proven to be very significant in the 2HDM mainly because of the presence of the charged Higgs boson. Various flavor observables like rare B decays, B meson mixing parameters, $\text{BR}(B \rightarrow X_s \gamma)$, LEP constraints on Z decay partial widths etc., which are sensitive to charged Higgs boson exchange, provide effective constraints on the available parameter space [34,35]. Here we take into account the decays $B \rightarrow X_s \gamma$ and $B_s \rightarrow \mu^+ \mu^-$, which are most constraining. This is done with the code `SuperIso` [23,24] where the model input is given by `2HDMC`. We have modified the code as to include the Higgs-Penguin type corrections in $B_s \rightarrow \mu^+ \mu^-$ which were not included in the original version of `SuperIso` [23,24]. These corrections are indeed relevant for the present work since these Higgs-Penguin contributions are the ones containing the potential effects from triple Higgs couplings in $B_s \rightarrow \mu^+ \mu^-$.

3 Triple Higgs couplings

In Ref. [9] several benchmark planes have been defined. Here we review the results for the $(c_{\beta-\alpha}, m_{H^\pm} = m_H = m_A \equiv m)$ plane in the 2HDM type I, with $\tan\beta = 10$ and m_{12}^2 fixed via Eq. (6). The allowed regions by the constraints considered are displayed in upper part of Fig. 1(A). The upper left panel shows the allowed regions by the collider searches and the direct measurements of the light 125 GeV Higgs boson, given by `HiggsBounds` and `HiggsSignals` respectively. The allowed region given by `HiggsSignals` is $\sim [-0.32, 0.28]$, nearly independent on m . The upper right panel shows the flavor constraints, that are not relevant for this choice of the input parameters. In the middle left plot the constraints from unitarity and stability are displayed, which are the most constraining ones. Positive and negative values for $c_{\beta-\alpha}$ are allowed for $m \lesssim 250$ GeV but above that mass, due to the stability conditions, only positive values for $c_{\beta-\alpha}$ up to $c_{\beta-\alpha} \sim 0.2$ are allowed. For masses larger than ~ 800 GeV both stability and unitarity conditions narrow the allowed region to the alignment limit. The middle right panel shows the final allowed region by all the

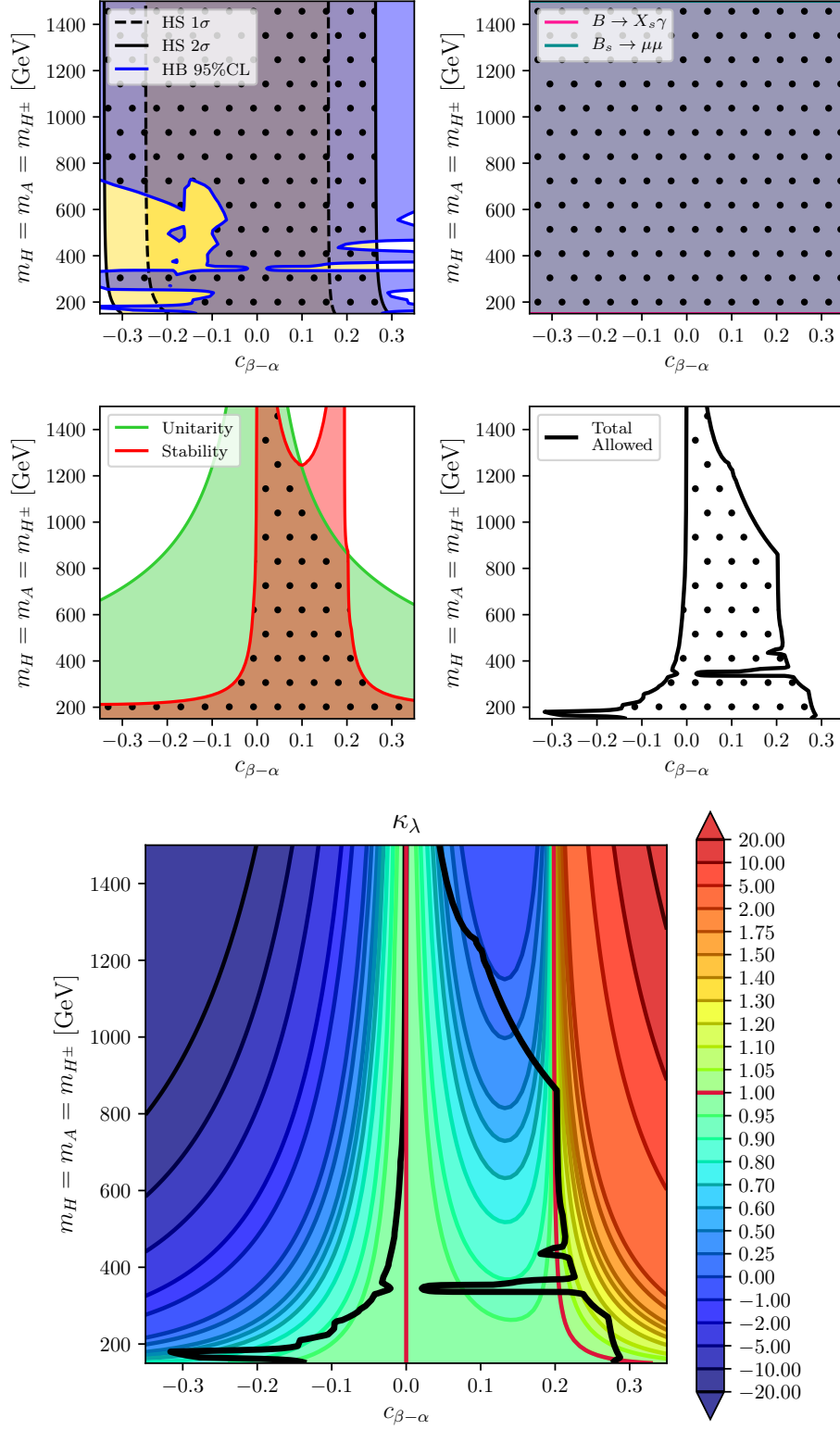


Figure 1: (A) Predictions for $\kappa_\lambda = \lambda_{hhh}/\lambda_{\text{SM}}$ in the 2HDM type I, scenario C, in the $(c_{\beta-\alpha}, m)$ plane with $m = m_H = m_A = m_{H^\pm}$, $m_{12}^2 = (m_H^2 \cos^2 \alpha)/(\tan \beta)$ and $\tan \beta = 10$. *Upper right plot:* Allowed areas by flavor physics from $B \rightarrow X_s \gamma$ (pink), $B_s \rightarrow \mu^+ \mu^-$ (teal) and both (dotted). *Middle left plot:* Allowed areas by the theoretical constraints from unitarity (green), stability (red) and both (dotted). *Middle right plot:* Total allowed area (dotted). *Lower big plot:* Contour lines of $\kappa_\lambda = \lambda_{hhh}/\lambda_{\text{SM}}$. Red contours correspond to $\kappa_\lambda = 1$. The thick solid contours is the boundary of the total allowed area.

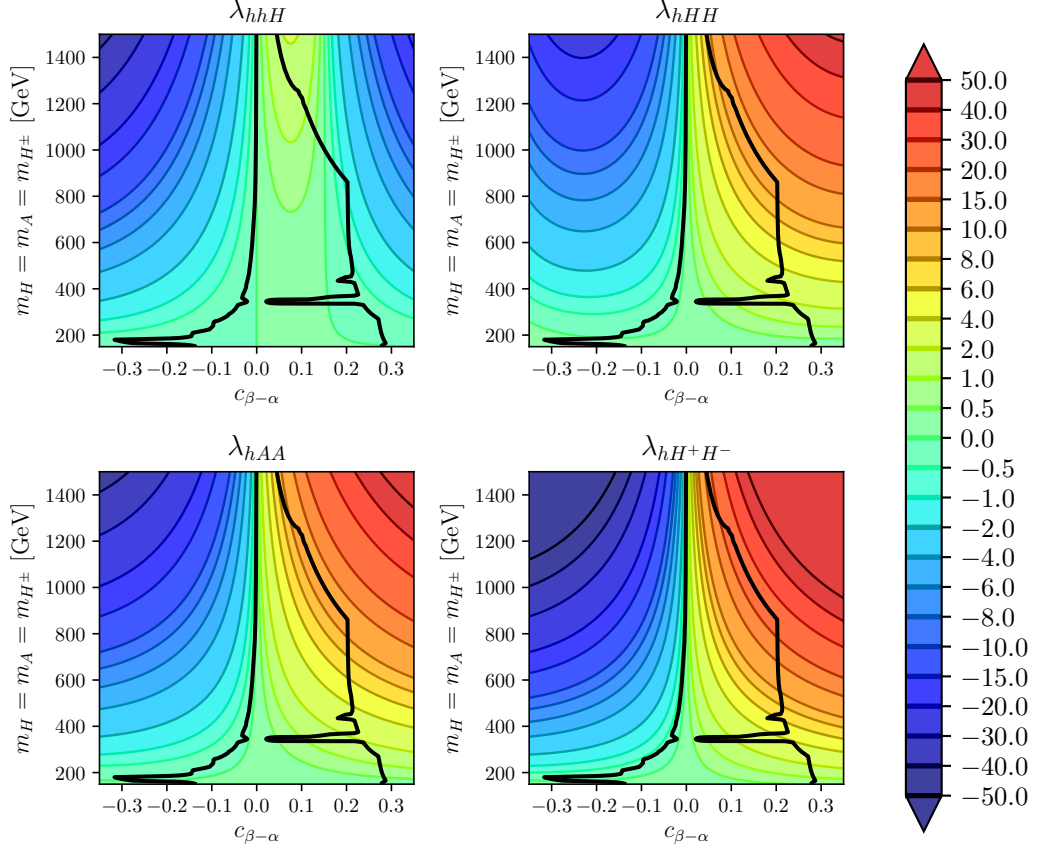


Figure 1: (B) Contour lines for triple Higgs couplings in the 2HDM type I, scenario C, in the $(c_{\beta-\alpha}, m)$ plane for $m = m_H = m_A = m_{H^\pm}$, $m_{12}^2 = (m_H^2 \cos^2 \alpha)/(\tan \beta)$ and $\tan \beta = 10$. *Upper left:* λ_{hhH} , *upper right:* λ_{hHH} , *lower left:* λ_{hAA} , *lower right:* $\lambda_{hH^+H^-}$. The thick solid contour is as in Fig. 1(A).

constrains discussed above, that is mainly dominated by the theoretical constraints. The corresponding (black) outline is shown in all other plots.

The predictions for the triple Higgs couplings with at least one h in this benchmark plane are displayed in the lower panel of Fig. 1(A) for κ_λ and in Fig. 1(B) in the case of λ_{hhH} (upper left), λ_{hHH} (upper right), λ_{hAA} (lower left) and $\lambda_{hH^+H^-}$ (lower right). The values that can be reached by κ_λ range from $\kappa_\lambda \sim 0.07$ for $c_{\beta-\alpha} \sim 0.1$ and large m_{H^\pm} close to 1200 GeV to about $\kappa_\lambda \sim 1.2$ for the largest allowed $c_{\beta-\alpha}$ values and $m_{H^\pm} \sim 300$ GeV. The values of λ_{hhH} range between ~ -1.0 and ~ 1.6 , where that maximum value of λ_{hhH} is found for $c_{\beta-\alpha} \sim 0.05$ and large m_{H^\pm} . Both κ_λ and λ_{hhH} tend to 1 and 0 respectively in the alignment limit.

The ranges reached by the triple Higgs couplings involving two heavy Higgs boson, as shown in Fig. 1(B), are found to be $\lambda_{hHH} \sim [-0.2, 12]$, $\lambda_{hAA} \sim [-0.2, 12]$ and $\lambda_{hH^+H^-} \sim [-0.5, 24]$. For all of them the maximum values are found on the edge for larger $c_{\beta-\alpha}$ and $800 \text{ GeV} \lesssim m_{H^\pm} \lesssim 1300 \text{ GeV}$.

In [9] we performed a thorough exploration of the five triple Higgs couplings that involves

	type I	type II
κ_λ	$[-0.5, 1.5]$	$[0.0, 1.0]$
λ_{hhH}	$[-1.4, 1.5]$	$[-1.6, 1.8]$
λ_{hHH}	$[0, 15]$	$[0, 15]$
λ_{hAA}	$[0, 16]$	$[0, 16]$
$\lambda_{hH^+H^-}$	$[0, 32]$	$[0, 32]$

Table 1: Final allowed ranges of κ_λ , λ_{hhH} , λ_{hHH} , λ_{hAA} and $\lambda_{hH^+H^-}$ by all the considered constraints in the 2HDM type I and type II.

at least one h state, and the final allowed ranges of those couplings are gathered in Tab. 1. The allowed range for κ_λ is smaller in type II compared to type I, because the collider measurements in type II are more stringent and require $c_{\beta-\alpha}$ to be closer to the alignment limit than for type I. For the other non-SM couplings the ranges are very similar in both type I and type II. Here it should be noted that the maximum values of λ_{hHH} , λ_{hAA} and $\lambda_{hH^+H^-}$ are realized in scenarios with mass splitting among the heavy Higgs bosons, i.e. in the cases (A) and (B), see Sect. 2.2. More details can be found in Ref. [9]. In particular, the large allowed ranges of κ_λ emphasize the importance of an evaluation of the sensitivity of future experiments (e^+e^- and pp) to λ_{hhh} away from its SM value.

4 Sensitivity at future e^+e^- colliders

In this section we discuss the impact of the studied triple Higgs couplings on the di-Higgs production at future linear e^+e^- colliders. We will consider two different channels: $e^+e^- \rightarrow h_i h_j Z$ and $e^+e^- \rightarrow h_i h_j \nu \bar{\nu}$ with $h_i h_j = hh, hH, HH$ and AA . The cross sections presented in this section were computed with **MadGraph** [36] and **FeynRules** [37], neglecting the electron mass. The width of the Higgs bosons in the 2HDM was computed with **2HDMC** [33].

We present in Fig. 2 an illustrative example of the results for the cross sections $e^+e^- \rightarrow h_i h_j Z$ (left) and $e^+e^- \rightarrow h_i h_j \nu \bar{\nu}$ (right) as a function of the collider energy. We chose a particular point of the 2HDM type I contained in the benchmark plane discussed in the previous section, with input parameters $m = 600$ GeV, $\tan \beta = 10$, $c_{\beta-\alpha} = 0.2$ and $m_{12}^2 = m_H^2 \cos^2 \alpha / \tan \beta$. For this point the following values for the triple Higgs couplings are realized: $\kappa_\lambda \simeq 1$, $\lambda_{hhH} = -0.5$, $\lambda_{hHH} = \lambda_{hAA} = 6$ and $\lambda_{hH^+H^-} = 12$. The value of $\kappa_\lambda \simeq 1$ away from the alignment limit is realized via “accidental” cancellations in the dependence of λ_{hhh} on the underlying parameters. One of the main differences between both channels is that all the cross sections in the $h_i h_j Z$ channel decrease with the center-of-mass energy \sqrt{s} , while in the case of $h_i h_j \nu \bar{\nu}$ the cross sections increase with \sqrt{s} (except for $hH\nu\bar{\nu}$ in the range of \sqrt{s} analyzed). The reason behind this is that the diagrams that contribute in the Z production channel are mediated by a Z^* , which decrease with the collision energy, but on the other hand in the neutrino channel there are diagrams mediated by a pair W^*W^* (known as vector boson fusion or VBF topologies) that are known to increase with the energy (see, e.g., Ref. [38] and references therein). This is indeed the reason why for e^+e^- colliders with

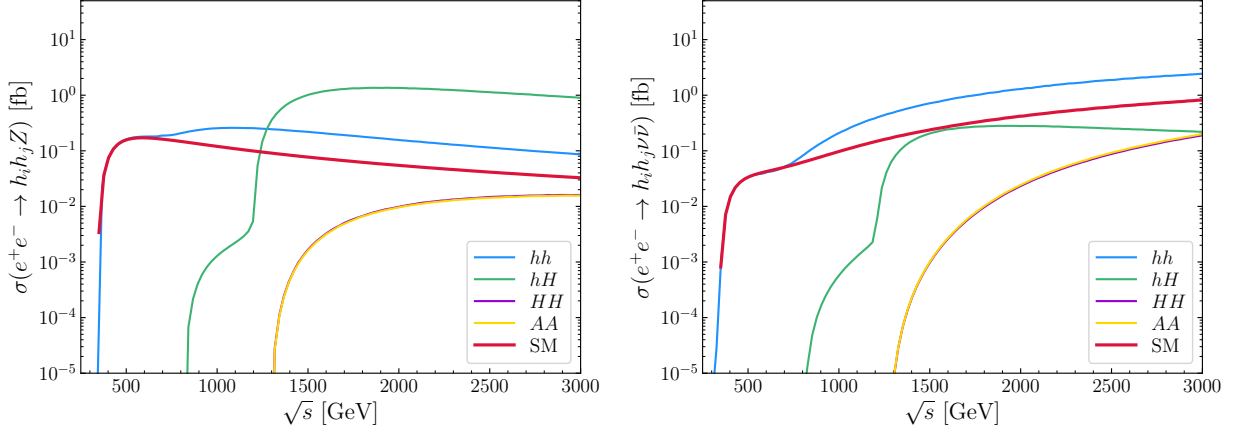


Figure 2: Cross sections as a function of the center-of-mass energy \sqrt{s} for the processes $e^+e^- \rightarrow h_i h_j Z$ (left) and $e^+e^- \rightarrow h_i h_j \nu \bar{\nu}$ (right) for the particular point of the 2HDM type I defined by the input parameter values: $m_H = m_A = m_{H^\pm} = 600$ GeV, $\tan \beta = 10$, $c_{\beta-\alpha} = 0.2$, and $m_{12}^2 = m_H^2 \cos^2 \alpha / \tan \beta$ (see text).

energies at and above the TeV scale the diagrams with VBF configuration dominates the $h_i h_j \nu \bar{\nu}$ production rates, even though the later also contains Z^* mediated diagrams.

The hh production in both channels (blue lines) shows an enhancement at $\sqrt{s} \gtrsim 700$ GeV with respect to the SM prediction (red lines). This difference can be explained with the new contributions coming from diagrams mediated by BSM Higgs bosons. The relevant BSM diagrams are $e^+e^- \rightarrow W^* W^* \nu \bar{\nu} \rightarrow H^{(*)} \nu \bar{\nu} \rightarrow hh \nu \bar{\nu}$ and $e^+e^- \rightarrow Z^* \rightarrow H^{(*)} Z \rightarrow hh Z (\rightarrow hh \nu \bar{\nu})$, that contain λ_{hhH} , as well as $e^+e^- \rightarrow Z^* \rightarrow h A^{(*)} \rightarrow hh Z (\rightarrow hh \nu \bar{\nu})$. All of them are resonant in the case that the (virtual) H^* or A^* propagates on-shell. The larger contribution of them is the one coming from H^* mediated diagrams, because the diagrams with a propagating A^* is proportional to the coupling $g_{hAZ} \propto c_{\beta-\alpha}$. Since the experimental data requires a SM-like h boson, one finds $c_{\beta-\alpha} \ll 1$, so that these are somewhat suppressed despite being resonant. It is important to note that in this case the narrow width approximation does not yield a good approximation to the total cross section, because the interference of this resonant diagrams with the rest of the contributions is not negligible.

In the case of the hHZ production (green line) we can see that the cross section can reach values around ~ 1 fb, more than one order of magnitude larger than $e^+e^- \rightarrow hhZ$ in the SM. However, the dominant contribution here is given by the resonant diagram $e^+e^- \rightarrow Z^* \rightarrow H A^{(*)} \rightarrow H h Z$, which does not depend on any triple Higgs coupling. A consequence of this is that the cross section receives a large enhancement around the threshold $\sqrt{s} \sim m_H + m_A = 1200$ GeV. This large contribution is also found in the process $e^+e^- \rightarrow hH \nu \bar{\nu}$, that shows the same behavior with \sqrt{s} as $e^+e^- \rightarrow hHZ$, but with a smaller cross section.

Finally, we comment the production of two heavy BSM bosons (purple lines for HH and yellow lines for AA). For our choice of $m_H = m_A$, the di- \mathcal{CP} -odd production is always very similar to the di- \mathcal{CP} -even production. (Consequently, the purple HH line is nearly fully covered by the yellow AA curve.) The HHZ and AAZ channels have a very small cross section, only reaching $\sim 10^{-2}$ fb at $\sqrt{s} = 3$ TeV. On the other hand, the HH/AA production

in the neutrino channel reaches sizable cross section, ~ 0.2 fb at 3 TeV, about the same level as the hH cross section. The $HH\nu\bar{\nu}$ and $AA\nu\bar{\nu}$ channels are mainly dominated by the diagram containing λ_{hHH} or λ_{hAA} , respectively.

5 Conclusions and summary

The measurement of the triple Higgs coupling λ_{hhh} is an important task at future colliders. Depending on its relative size to the SM value, certain collider options result in a higher (or lower) experimental accuracy. On the other hand, large values of triple Higgs couplings involving heavy Higgs bosons can lead to relevant effects on the production cross sections of BSM Higgs bosons.

Within the framework of Two Higgs Doublet Models (2HDM) type I and II we have reviewed the allowed ranges for all triple Higgs couplings involving at least one light, SM-like Higgs boson [9]. All relevant theoretical and experimental constraints are taken into account. This comprises from the theory side unitarity and stability conditions. From the experimental side we require agreement with measurements of the SM-like Higgs-boson rate as measured at the LHC as well as with the direct BSM Higgs-boson searches. Furthermore agreement with flavor observables and electroweak precision data (where the T parameter plays the most important role) was required. We have shown one benchmark plane as example. Taking all analyzed benchmark planes into account [9], the final allowed ranges for the triple Higgs couplings are obtained; they are summarized in Tab. 1.

We have also studied how these triple Higgs couplings can affect the neutral di-Higgs production at future e^+e^- colliders in two different production modes: $e^+e^- \rightarrow h_i h_j Z$ and $e^+e^- \rightarrow h_i h_j \nu\bar{\nu}$ with $h_i h_j = hh, hH, HH, AA$. In an example point, allowed by all the relevant constraints (and part of the benchmark plane shown), we find clear signals of BSM Higgs bosons, arising from the studied triple Higgs couplings. We find that the production of hh can be affected by λ_{hHH} via the resonant processes $e^+e^- \rightarrow W^*W^*\nu\bar{\nu} \rightarrow H^{(*)}\nu\bar{\nu} \rightarrow hh\nu\bar{\nu}$. The Z channel will be important at lower collider energies, such like ILC, and will be able to give access to this coupling if the mass of H is sufficiently low to be produced on-shell (a viable possibility in the 2HDM). On the other hand, the neutrino channel will be dominant and will have a larger cross section at higher center-of-mass energies projected for CLIC. In this case, the $hh\nu\bar{\nu}$ channel can give access to λ_{hHH} for larger values for m_H . In the presented point the deviation from the SM of the h self-coupling, given by $\kappa_\lambda := \lambda_{hhh}/\lambda_{hhh}^{\text{SM}}$, is very small due to an “accidental” cancellations in the dependence of λ_{hhh} on the underlying parameters. As a consequence the effect of this parameter and the corresponding diagrams are very similar to the SM case. Analyses of the accuracy of the measurement of λ_{SM} have been performed, see for instance Refs. [38, 39] and references therein, and a similar accuracy can be expected the case of the 2HDM. The hH production channels do not show any important dependence on any of the triple Higgs couplings. On the other hand, the production cross sections of $HH\nu\bar{\nu}$ and $AA\nu\bar{\nu}$ (which are very similar), are dominated by the size of λ_{hHH} or λ_{hAA} , respectively. Therefore, a measurement of these processes would yield a good opportunity to measure these couplings.

References

- [1] G. Aad *et al.* [ATLAS Collaboration], Phys. Lett. B **716** (2012) 1 [arXiv:1207.7214 [hep-ex]].
- [2] S. Chatrchyan *et al.* [CMS Collaboration], Phys. Lett. B **716** (2012) 30 [arXiv:1207.7235 [hep-ex]].
- [3] G. Aad *et al.* [ATLAS and CMS Collaborations], JHEP **1608** (2016) 045 [arXiv:1606.02266 [hep-ex]].
- [4] J. de Blas, M. Cepeda, J. D’Hondt, R. Ellis, C. Grojean, B. Heinemann, F. Maltoni, A. Nisati, E. Petit, R. Rattazzi and W. Verkerke, JHEP **01** (2020), 139 [arXiv:1905.03764 [hep-ph]].
- [5] J. Alison *et al.*, [arXiv:1910.00012[hep-ph]].
- [6] J. F. Gunion, H. E. Haber, G. L. Kane and S. Dawson, Front. Phys. **80** (2000), 1-404, SCIPP-89/13. Erratum: [arXiv:hep-ph/9302272 [hep-ph]].
- [7] M. Aoki, S. Kanemura, K. Tsumura and K. Yagyu, Phys. Rev. D **80**, 015017 (2009) [arXiv:0902.4665 [hep-ph]].
- [8] G. C. Branco, P. M. Ferreira, L. Lavoura, M. N. Rebelo, M. Sher and J. P. Silva, Phys. Rept. **516** (2012) 1 [arXiv:1106.0034 [hep-ph]].
- [9] F. Arco, S. Heinemeyer and M. J. Herrero, Eur. Phys. J. C **80** (2020) no.9, 884 [arXiv:2005.10576 [hep-ph]].
- [10] S. L. Glashow and S. Weinberg, Phys. Rev. D **15**, 1958 (1977).
- [11] N. G. Deshpande and E. Ma, Phys. Rev. D **18** (1978) 2574.
- [12] G. Bhattacharyya and D. Das, Pramana **87** (2016) no.3, 40 [arXiv:1507.06424 [hep-ph]].
- [13] A. G. Akeroyd, A. Arhrib and E. M. Naimi, Phys. Lett. B **490** (2000) 119 [hep-ph/0006035].
- [14] A. Barroso, P. M. Ferreira, I. P. Ivanov and R. Santos, JHEP **1306** (2013) 045 [arXiv:1303.5098 [hep-ph]].
- [15] P. Bechtle, O. Brein, S. Heinemeyer, G. Weiglein and K. E. Williams, Comput. Phys. Commun. **181** (2010) 138 [arXiv:0811.4169 [hep-ph]].
- [16] P. Bechtle, O. Brein, S. Heinemeyer, G. Weiglein and K. E. Williams, Comput. Phys. Commun. **182** (2011) 2605 [arXiv:1102.1898 [hep-ph]].
- [17] P. Bechtle, O. Brein, S. Heinemeyer, O. Stål, T. Stefaniak, G. Weiglein and K. E. Williams, Eur. Phys. J. C **74** (2014) no.3, 2693 [arXiv:1311.0055 [hep-ph]].

- [18] P. Bechtle, S. Heinemeyer, O. Stål, T. Stefaniak and G. Weiglein, Eur. Phys. J. C **75** (2015) no.9, 421 [arXiv:1507.06706 [hep-ph]].
- [19] P. Bechtle, D. Dercks, S. Heinemeyer, T. Klingl, T. Stefaniak, G. Weiglein and J. Wittbrodt, [arXiv:2006.06007 [hep-ph]].
- [20] P. Bechtle, S. Heinemeyer, O. Stål, T. Stefaniak and G. Weiglein, Eur. Phys. J. C **74** (2014) no.2, 2711 [arXiv:1305.1933 [hep-ph]].
- [21] P. Bechtle, S. Heinemeyer, O. Stål, T. Stefaniak and G. Weiglein, JHEP **1411** (2014) 039 [arXiv:1403.1582 [hep-ph]].
- [22] P. Bechtle, S. Heinemeyer, T. Klingl, T. Stefaniak, G. Weiglein and J. Wittbrodt, Eur. Phys. J. C **81** (2021) no.2, 145 [arXiv:2012.09197 [hep-ph]].
- [23] F. Mahmoudi, Comput. Phys. Commun. **180** (2009) 1579 [arXiv:0808.3144 [hep-ph]].
- [24] F. Mahmoudi, Comput. Phys. Commun. **180** (2009), 1718-1719.
- [25] X. Q. Li, J. Lu and A. Pich, JHEP **1406** (2014) 022 [arXiv:1404.5865 [hep-ph]].
- [26] X. D. Cheng, Y. D. Yang and X. B. Yuan, Eur. Phys. J. C **76** (2016) no.3, 151 [arXiv:1511.01829 [hep-ph]].
- [27] P. Arnan, D. Becirevic, F. Mescia and O. Sumensari, Eur. Phys. J. C **77** (2017) no.11, 796 [arXiv:1703.03426 [hep-ph]].
- [28] M. E. Peskin and T. Takeuchi, Phys. Rev. Lett. **65** (1990) 964.
- [29] M. E. Peskin and T. Takeuchi, Phys. Rev. D **46** (1992) 381.
- [30] W. Grimus, L. Lavoura, O. M. Ogreid and P. Osland, J. Phys. G **35** (2008) 075001 [arXiv:0711.4022 [hep-ph]].
- [31] G. Funk, D. O’Neil and R. M. Winters, Int. J. Mod. Phys. A **27** (2012) 1250021 [arXiv:1110.3812 [hep-ph]].
- [32] M. Tanabashi *et al.* [Particle Data Group], Phys. Rev. D **98** (2018) no.3, 030001.
- [33] D. Eriksson, J. Rathsman and O. Stål, Comput. Phys. Commun. **181** (2010) 189 [arXiv:0902.0851 [hep-ph]].
- [34] T. Enomoto and R. Watanabe, JHEP **1605** (2016) 002 [arXiv:1511.05066 [hep-ph]].
- [35] A. Arbey, F. Mahmoudi, O. Stål and T. Stefaniak, Eur. Phys. J. C **78** (2018) no.3, 182 [arXiv:1706.07414 [hep-ph]].
- [36] J. Alwall, R. Frederix, S. Frixione, V. Hirschi, F. Maltoni, O. Mattelaer, H. S. Shao, T. Stelzer, P. Torrielli and M. Zaro, JHEP **07** (2014), 079 [arXiv:1405.0301 [hep-ph]].
- [37] A. Alloul, N. D. Christensen, C. Degrande, C. Duhr and B. Fuks, Comput. Phys. Commun. **185** (2014) 2250 [arXiv:1310.1921 [hep-ph]].

- [38] P. Roloff *et al.* [CLICdp], Eur. Phys. J. C **80** (2020) no.11, 1010 [arXiv:1901.05897 [hep-ex]].
- [39] M. Gonzalez-Lopez, M. J. Herrero and P. Martinez-Suarez, Eur. Phys. J. C **81** (2021) no.3, 260 [arXiv:2011.13915 [hep-ph]].